

Quantum non-Gaussian Photon Coincidences

Luk Lachman* and Radim Filip†

Department of Optics, Faculty of Science, Palacký University,
17. listopadu 1192/12, 771 46 Olomouc,
Czech Republic

Photon coincidences represent an important resource for quantum technologies. They expose nonlinear quantum processes in matter and are essential for sources of entanglement. We derive broadly applicable criteria for quantum non-Gaussian two-photon coincidences that certify a new quality of photon sources. The criteria reject states emerging from Gaussian parametric processes, which often limit applications in quantum technologies. We also analyse the robustness of the quantum non-Gaussian coincidences and compare with the heralded quantum non-Gaussianity of single-photons based on them.

Five decades ago, coincidences detected in photon-counting experiments initiated the first fundamental tests of nonclassical photon pairs from nonlinear processes [1–5]. These photon pairs were used to produce photon entanglement in different degrees of freedom [6, 7]. After two decades, the effort move on to entanglement-based quantum key distribution at a significant distance and in real optical networks [8]. Recently, superconducting counters of itinerant microwave photons [9–11] also allowed observation of nonclassical coincidences. This initiated the study of integrated superconducting microwave photonics beyond hybridisation in a single system [12–15]. Simultaneously, the correlation between optical or microwave photons and excitations in atomic [16–19], solid-state [20–22], superconducting [23] and mechanical systems [24, 25] established a new hybrid quantum physics. A violation of Bell inequalities over a distance has already been confirmed [26], which aims for device-independent secure key distribution [27, 28]. Therefore, photon coincidences and their analysis are crucial for the further development of many current and future experiments.

For a long time, nonclassical photon coincidences have been in the main focus, as they are necessary conditions for many quantum phenomena and applications. The photon pairs produced by spontaneous parametric down-conversion, optical parametric oscillators and similar processes were the principal sources. However, the photon coincidences from such Gaussian processes still exhibit *multiphoton* components. This unwanted contribution grows with increasing pumping of the Gaussian process. It is known that they represent limiting factors for the rate and security of quantum key distribution [29]. Despite some solutions for particular applications, multiphoton contributions generally restrict the speed and performance of any entanglement-based photonic protocols, which already achieve a considerable distance [30]. The states with reduced multiphoton contributions will expand current photonic quantum technology. Currently

developing experimental platforms brought new versions of two-photon optical processes in atoms [31, 32] and solid-state systems [33–36] with rapid advances [37–45], but also with single-atom mechanical oscillators [46–48] and at microwave frequencies [48] and soon in other superconducting circuits [49]. This effort even extends to observable three-photon coincidences [50]. They are all capable of producing photon pairs with much lower multiphoton contributions than Gaussian processes.

These experimental developments allow us to test, for the first time, that they conclusively reach the capability to produce *quantum non-Gaussian coincidences* that are better than coincidences provided by any correlated Gaussian states of light. The eminent first target is a coincidence of Fock states $|1\rangle|1\rangle$ in two different modes without any higher photon contribution. As described above, it is ideal for building two-photon entanglement without multiphoton components, but also other applications in multiplexing of Fock-state-based quantum sensing [51]. In this Letter, we derive ab initio criteria for quantum non-Gaussian coincidences for commonly used experimental setups with multiplexed single-photon detectors, analyse their essential features and robustness and modify the method for currently developing photon number detectors. Remarkably, low photon rates do not preclude observation of quantum non-Gaussian coincidences. Therefore they are applicable to the majority of above mentioned experimental platforms even at an early stage of their development. This result qualitatively extends the already experimentally verified quantum non-Gaussian statistics of heralded single-mode states [52]. The quantum non-Gaussianity was also recognized in light from quantum dots [53], which have the potential to test quantum non-Gaussian coincidences. Therefore, we can compare these two different quantum non-Gaussian statistics of photons. Since nonclassicality is a necessary condition of the quantum non-Gaussianity, we analyse both quantum non-Gaussian statistics of photons in the experimental layout where nonclassical coincidences are detected [37] to understand the difference from the standard nonclassical tests.

Nonclassical photon coincidences—A response of a detector rejecting classically correlated classical waves sig-

* lachman@optics.upol.cz

† filip@optics.upol.cz

nifies nonclassical photon coincidences. Particularly, the nonclassical coincidences manifest themselves in a minimal layout depicted in Fig. 1a) where the simultaneous click of two of four detectors can be measured. Light in two distinguishable modes denoted as 1 and 2 propagates through a beam-splitter (BS) in each mode and two pairs of single-photon avalanche diodes (SPADs) measure the split light. A criterion compares probabilities of coincidences at selected detectors as summarized in Fig. 1b). A success probability P_s quantifies events when the detectors $SPAD_{a,1}$ and $SPAD_{a,2}$ click simultaneously. The error probability $P_{e,i}$ with $i = 1, 2$ measures when the detectors $SPAD_{a,i}$ and $SPAD_{b,i}$ click. Thus, the success events represent coincidences occurring in different modes and error events correspond to coincidences in the same mode. The involved error probabilities allow us to exploit the criterion to experimentally test emission processes even with low rates. The criterion stems from a linear combination of the probabilities

$$F_a(\rho) = P_s + a(P_{e,1} + P_{e,2}), \quad (1)$$

where a is a free parameter. To achieve the nonclassicality criterion for such measurement, the function $F_a(\rho)$ is optimized over all classical states

$$\rho \neq \int P(\alpha_1, \alpha_2) |\alpha_1\rangle_1 \langle \alpha_1| \otimes |\alpha_2\rangle_2 \langle \alpha_2| d^2\alpha_1 d^2\alpha_2, \quad (2)$$

where $P(\alpha, \beta)$ is a density probability function and subscripts 1 and 2 distinguish the two modes. Optimizing the functional (1) over classical states leads to a threshold function $F(a)$, on which the criterion imposes a condition $\exists a : F_a(\rho) > F(a)$ [54]. Exclusion of the parameter a from the criterion induces an inequality

$$\frac{2P_s}{P_{e,1} + P_{e,2}} > 1 \quad (3)$$

giving a condition for nonclassicality on the measurable quantities. Simultaneous generation of pairs $|1, 1\rangle$ of single-photon states without any multiphoton contributions will always be detected as nonclassical. Violation $P_s^2/(P_{e,1}P_{e,2}) \leq 1$ [5] from the Cauchy-Schwarz inequality reveals the nonclassicality identically for those ideal cases. Both conditions remain the same even for more realistic states producing the error events if both modes are occupied symmetrically, i. e. $P_{e,1} = P_{e,2}$. However, the condition (3) gets stricter for states contributing asymmetrically to the error event. To continue tests of fundamental aspects of the photon pairs and its generation, the threshold needs to be moved up to reject all two-mode Gaussian states from parametric processes governed by the quadratic interaction Hamiltonians.

Quantum non-Gaussian photon coincidences— States beyond mixtures of Gaussian states exhibit more profound quantum aspects than nonclassical light. Quantum non-Gaussian photon coincidences identify such states occupying several modes, and therefore they reject even

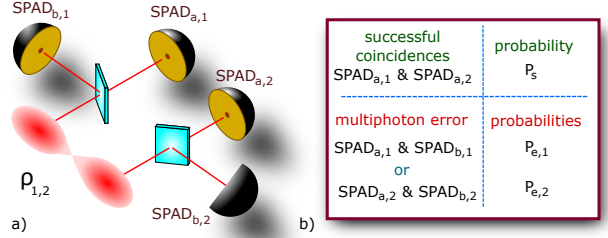


FIG. 1. a) A scheme enabling detection of the nonclassical and quantum non-Gaussian two-photon coincidences. Both optical modes are split by a balanced BS and measured by two pairs of SPADs. The criteria for both quantum features explore the relation between coincidences happening in different modes (success) or in the same mode (error). b) The coincidences relevant for success and error probabilities are outlined.

states exhibiting Gaussian photon correlations. Let us focus on the manifestation of that quantum aspect on the layout in Fig. 1a) again. To obtain a threshold for quantum non-Gaussian coincidences, we use a pure Gaussian state defined by Gaussian unitary operations acting on the vacuum [55]. For the two-mode cases considered, the Gaussian state $|G\rangle_{1,2}$ has the form [56]

$$|G\rangle_{1,2} = D_1(\alpha_1) D_2(\alpha_2) U_{BS}(\tau) S_1(\xi_1) S_2(\xi_2) |0\rangle_1 |0\rangle_2, \quad (4)$$

where $S_i(\xi) = \exp \left[\xi \left(a_i^\dagger \right)^2 - \xi^* a_i^2 \right]$ is the squeezing operator, $D_i(\alpha) = \exp \left(\alpha a_i^\dagger - \alpha^* a_i \right)$ is the displacement operator and $U_{BS}(\tau) = \exp \left(\tau a_1^\dagger a_2 - \tau^* a_1 a_2^\dagger \right)$ corresponds to a unitary operator describing the interference on a beam-splitter. Thus, the quantum non-Gaussian coincidences reject all mixtures of the state $|G\rangle_{1,2}$, i. e.

$$\rho \neq \int P(G) |G\rangle_{1,2} \langle G| d^2\alpha_1 d^2\alpha_2 d^2\xi_1 d^2\xi_2 d\tau, \quad (5)$$

where the function $P(G)$ is a density probability function of the vector G of complex parameters $\alpha_{1,2}$, $\xi_{1,2}$ and τ identifying a Gaussian state $|G\rangle_{1,2}$. It imposes stricter demands on the coincidences than the nonclassical condition (3) because it also rejects states with a Gaussian correlation of photons typical for linearized dynamics from quadratic nonlinearities. Recognition of quantum non-Gaussian coincidences provides a criterion that is derived analogously to the nonclassicality condition. The optimal state is $|G\rangle_{1,2}$ due to the linearity of the function $F_a(\rho)$ [57]. A challenging task is to find the unitary operators in (4) producing the optimal state. Its parameters are guessed to be $\alpha_i = 0$, $\tau = \pi/4$ and $\xi_2 = -\xi_1 = \xi$ with ξ being real, which defines a state

$$|G_r\rangle_{1,2} = \sqrt{1-r^2} \sum_{n=0}^{\infty} r^n |n\rangle |n\rangle, \quad (6)$$

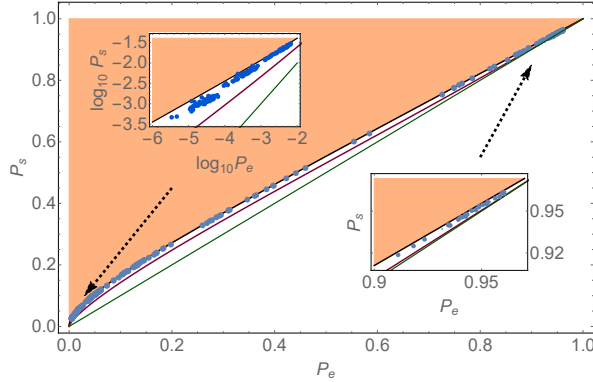


FIG. 2. The quantum non-Gaussian coincidences are recognized when the measured probabilities P_s and P_e belong to the orange region. The solid black line corresponds to the threshold determined by relation (7). Its reliability was verified by a Monte-Carlo simulation producing in total 10^7 random Gaussian states, see the Supplemental Material for more details. Five hundred best attempts are depicted by the blue points. The purple line shows a threshold for two factorizable Gaussian states to visualize that states with Gaussian photon correlation can be above them. The green line corresponds to the threshold of nonclassicality (3). The upper inset presents the thresholds and results of the Monte-Carlo simulation in a region of very attenuated states which is relevant for many experiments [58]. The lower inset zooms the results in the corner with very high probabilities of success and error.

where $r = (1 - e^{-2\xi})/(1 + e^{-2\xi})$. A Monte-Carlo simulation certified this state is optimal. Fig. 2 shows outputs of the simulation and the Supplemental Material provides more details about it. The threshold implied by the optimal state (6) reads

$$P_s > \frac{1}{2} \sqrt{\frac{P_e}{8 + P_e}} \left[2 + P_e + \sqrt{P_e(8 + P_e)} \right], \quad (7)$$

where P_e denotes the average of error probabilities, i. e. $P_e = (P_{e,1} + P_{e,2})/2$. All the simulated states $|G\rangle_{1,2}$ were covered by the threshold (7). Thus, only states (5) can surpass the threshold. In Fig. 2, we compare criterion (3) in green with the criterion for quantum non-Gaussian coincidences (7) in black. The figure also compares these thresholds with a line covering all mixtures of factorized Gaussian states. It highlights that states with Gaussian correlations establish the condition on quantum non-Gaussian coincidences. Importantly, the criteria behave differently for a large class of experimentally relevant states with $P_e \ll 1$. Whereas rejection of all factorized Gaussian states in this region demands $P_s^3 \gtrsim P_e^2/2$, quantum non-Gaussian coincidences require $P_s^2 \gtrsim P_e/8$ representing a stricter condition. The demands of the criteria (7) and (3) can be analyzed on a particular model of experimentally relevant states. It also allows us to explore how quantum non-Gaussianity manifests itself in that state in other layouts and compare it with quantum non-Gaussian coincidences as presented later.

Testing experimental example— Solid state sources ex-

ploit a cascade energy transfer in matter to radiate a correlated pair of photons [36, 45]. Typically, such a source suffers from high losses and background noise deteriorating the photon statistics and a density matrix of the radiated light approaches

$$\rho = \rho_{\eta,T} \otimes \tilde{\rho}_1(T\bar{n}) \otimes \tilde{\rho}_2(T\bar{n}), \quad (8)$$

where $\tilde{\rho}_i(T\bar{n})$ is the background noise in the i th mode obeying the Poissonian photon distribution with the mean number of photons $T\bar{n}$. The state $\rho_{\eta,T}$ reads

$$\begin{aligned} \rho_{\eta,T} = & \eta T^2 |1,1\rangle\langle 1,1| \\ & + \eta T(1-T)(|1,0\rangle\langle 1,0| + |0,1\rangle\langle 0,1|) \\ & + [(1-\eta) + \eta(1-T)^2] |0,0\rangle\langle 0,0|, \end{aligned} \quad (9)$$

where η is the probability that a photon pair $|1,1\rangle$ is generated and T quantifies the optical losses together with the quantum efficiency of the SPADs. Both the losses and the background noise reduce the coincidences, i. e. the component $|1,1\rangle$. Considering a limit of states with strongly suppressed multiphoton contributions, the success probability is $P_s \approx T^2 [\eta + \bar{n}^2 + \eta\bar{n}(2-T)]/4$ and the error probability approaches $P_e \approx \eta T^2 \bar{n} + T^2(2 - 3\eta T)\bar{n}^2/4$, where we assume $\bar{n} \ll 1$ without any conjecture about losses T and the parameter η . The Supplemental Material involves formulas expressing these probabilities beyond the approximation. According to them, the considered state exhibits the nonclassicality for arbitrary noise if $\eta T > 0$. Thus, nonclassical photon coincidences impose no condition on the states (8). In contrast, the quantum non-Gaussian coincidences are observed only for some states with the form (8). Analytical conditions on the state are derived only for the considered limit. Employing relations approximating the measured probabilities and the approximate threshold $P_s^2 \approx P_e/8$, gives rise to an approximate condition

$$\eta \gtrsim \frac{1}{2T^2} (1 + \sqrt{1 + 2T^2}) \bar{n}. \quad (10)$$

It shows how this quantum aspect is sensitive to the noise contributions in this regime. Expressing T from formula (10) estimates how much loss the criterion (7) tolerates. It gives rise to the relation

$$T \approx \left[\frac{\bar{n}(2\eta + \bar{n})}{2\eta^2} \right]^{1/2}, \quad (11)$$

which quantifies approximate robustness against loss. Considering the results in [52], it represents a depth of quantum non-Gaussian coincidences. The Supplemental Material provides numerical results showing accurately when the considered state manifests the quantum non-Gaussian coincidences.

Heralded and unheralded single-mode quantum non-Gaussianity— The presented quantum non-Gaussian coincidences can be applied to prepare a non-Gaussian single-photon state in a single-mode [52]. In that case,

the detection exploits a BS that directs the light towards two SPADs. The setup in Fig. 1 can be modified for detecting unheralded quantum non-Gaussianity by ignoring the response of $\text{SPAD}_{a,2}$ and $\text{SPAD}_{b,2}$, which measure the same mode. Alternatively, these detectors can be used to herald the preparation of a measured state in the first mode. In both cases, the criterion imposes a condition on outputs of the remaining pair of the detectors $\text{SPAD}_{a,1}$ and $\text{SPAD}_{b,1}$. The condition is derived in Ref. [59]. Thus, quantum non-Gaussian coincidences can be compared with the manifestation of the heralded and unheralded quantum non-Gaussianity in a single-mode by the model state (9). The reduced density matrix of the unheralded state reads

$$\rho_r = [\eta T |1\rangle\langle 1| + (1 - \eta T) |0\rangle\langle 0|] \otimes \tilde{\rho}(T\bar{n}) \quad (12)$$

with $\tilde{\rho}$ standing for the density matrix of the Poissonian noise. In the other scenario, the neglected pair of the SPADs is employed for preparation of a heralded state [60]. Then, the heralded quantum non-Gaussianity is exhibited by a state

$$\rho_h = \rho_{h,s} \otimes \tilde{\rho}(T\bar{n}), \quad (13)$$

where the single-photon component obtains

$$\begin{aligned} \rho_{h,s} = \frac{1}{N} & [(1 - \eta T)(1 - e^{-T\bar{n}}) + \eta T(1 - T)e^{-T\bar{n}}] |0\rangle\langle 0| \\ & + \frac{1}{N} \eta T e^{-T\bar{n}} (-1 + e^{T\bar{n}} + T) |1\rangle\langle 1| \end{aligned} \quad (14)$$

with $N = 1 - e^{-T\bar{n}} + e^{-T\bar{n}}\eta T$ being the probability of the heralded events. Let us inspect the conditions of the heralded and unheralded single-mode quantum non-Gaussianity in a region of states with very low noise contributions $\bar{n} \ll 1$. The approximate criterion obtains the form $P_s^3 > P_e/4$ where P_s denotes a probability of a click occurring on $\text{SPAD}_{a,1}$ and P_e stands for a probability identical to error probability $P_{e,1}$ introduced for detecting quantum non-Gaussian photon coincidences. The test of quantum non-Gaussianity requires [59]

$$\eta > \sqrt{\bar{n}/T} \quad (15)$$

for the unheralded case. Comparing relations (10) and (11) shows that quantum non-Gaussian photon coincidences survive lower photon-pair emission η but they are more sensitive to losses than unheralded single-mode quantum non-Gaussianity [61]. When heralding is used for a state preparation, the quantum non-Gaussianity of heralded states manifests itself when $T > \bar{n}$ regardless of the parameter η [52]. Therefore, the single-mode quantum non-Gaussianity is revealed more easily on heralded states (8) than the quantum non-Gaussian coincidences. However, the heralding on states from Gaussian parametric processes can generate quantum non-Gaussianity as well [52]. The Supplemental Material presents accurate evaluation of the quantum non-Gaussianity beyond the approximate regime for both detection scenarios.

Quantum non-Gaussian coincidences for detection with PNRDs— The layout in Fig. 1 can be modified for recognition of the quantum non-Gaussian coincidences employing photon-number resolving detectors (PNRDs) instead of SPADs. A PNRD allows us to distinguish the number of arriving photons. Two PNRDs responding on different modes quantify the probability $P_{m,n} = \langle m|\langle n|\rho|n\rangle|m\rangle$. Following the approach, we define the success probability by $P_s = P_{1,1}$. The error probability $P_{e,i}$ corresponds to probability of multiphoton contributions in the i th mode, i. e. $P_{e,i} = 1 - P_0^{(i)} - P_1^{(i)}$, where $P_n^{(i)}$ is the photon number distribution in the i th mode with the other mode being ignored. The state (6) establishes a criterion of quantum non-Gaussian coincidences in the form

$$P_s > \sqrt{P_e} - P_e \quad (16)$$

in this detection scheme, where P_e stands for the average of error probabilities again. The covering of all mixtures of Gaussian states was verified by a Monte-Carlo simulation as well. Applicability of the criterion (16) can be illustrated on the example of the model state (8). Assuming the limit of states with $\bar{n} \ll 1$ leads to conditions imposed on such model states, which are identical with relations (10) and (11) following from the criterion (7). Beyond that limit, the conditions differentiate, see the Supplemental Material for more details. Thus, the criterion (16) can be used specifically for two-quanta experiments where two-mode photon number statistics is detectable using optical homodyne tomography [62], in microwave experiments [63] and trapped ions experiments [46, 47].

Conclusion and outlook— We extended quantum non-Gaussianity of single mode states [64] to quantum non-Gaussian coincidences between two modes of light, microwaves or phonons of mechanical oscillators. The proposed methods are directly applicable to the two-mode versions of optical experiments with atomic systems [31, 32], two-photon solid-state emitters [38–43], but also to upcoming electromechanical experiments [65, 66], quantum mechanics with trapped ions [46, 47] and two-mode superconducting circuits [63, 67]. A straightforward theoretical extension is evaluation of the multiphoton quantum non-Gaussian coincidences of Fock states $|n\rangle|m\rangle$ to investigate multiphoton and multiphonon nonlinear process. It can be applied to time-bin experiments with single-photon guns to test prepared coincidences [68–71]. Simultaneously, the approach can be extended to exposing the quantum non-Gaussianity of sources producing triplets of photons [50].

ACKNOWLEDGMENTS

We thank Darren W. Moore for a fruitful discussion. We acknowledge the support from the Czech Science Foundation under the project 20-16577S. This work has

received national funding from the MEYS and the funding from European Unions Horizon 2020 (2014-2020) research and innovation framework programme under grant agreement No 731473 (project 8C18002). Project HYPER-U-P-S has received funding from the Quan-

tERA ERA-NET Cofund in Quantum Technologies implemented within the European Unions Horizon 2020 Programme. R.F. acknowledges project LTAUSA19099 from the Ministry of Education, Youth and Sports of Czech Republic.

[1] J. F. Clauser, *Physical Review D* **9**, 853 (1974).

[2] E. S. Fry and R. C. Thompson, *Physical Review Letters* **37**, 465 (1976).

[3] A. Aspect, P. Grangier, and G. Roger, *Physical Review Letters* **49**, 91 (1982).

[4] S. Friberg, C. K. Hong, and L. Mandel, *Physical Review Letters* **54**, 2011 (1985).

[5] A. Kuzmich, W. P. Bowen, A. D. Boozer, A. Boca, C. W. Chou, L.-M. Duan, and H. J. Kimble, *Nature* **423**, 731 (2003).

[6] P. G. Kwiat, E. Waks, A. G. White, I. Appelbaum, and P. H. Eberhard, *Physical Review A* **60**, R773 (1999).

[7] J. Brendel, N. Gisin, W. Tittel, and H. Zbinden, *Physical Review Letters* **82**, 2594 (1999).

[8] F. Xu, X. Ma, Q. Zhang, H.-K. Lo, and J.-W. Pan, *Reviews of Modern Physics* **92**, 025002 (2020).

[9] Y.-F. Chen, D. Hover, S. Sendelbach, L. Maurer, S. T. Merkel, E. J. Pritchett, F. K. Wilhelm, and R. McDermott, *Physical Review Letters* **107**, 217401 (2011).

[10] J.-C. Besse, S. Gasparinetti, M. C. Collodo, T. Walter, P. Kurpiers, M. Pechal, C. Eichler, and A. Wallraff, *Physical Review X* **8**, 021003 (2018).

[11] P. Kurpiers, P. Magnard, T. Walter, B. Royer, M. Pechal, J. Heinsoo, Y. Salathé, A. Akin, S. Storz, J.-C. Besse, S. Gasparinetti, A. Blais, and A. Wallraff, *Nature* **558**, 264 (2018).

[12] T. Brecht, W. Pfaff, C. Wang, Y. Chu, L. Frunzio, M. H. Devoret, and R. J. Schoelkopf, *npj Quantum Information* **2**, 021003 (2016).

[13] T. Brecht, Y. Chu, C. Axline, W. Pfaff, J. Blumoff, K. Chou, L. Krayzman, L. Frunzio, and R. Schoelkopf, *Physical Review Applied* **7**, 044018 (2017).

[14] L. Fan, C.-L. Zou, R. Cheng, X. Guo, X. Han, Z. Gong, S. Wang, and H. X. Tang, *Science Advances* **4**, eaar4994 (2018).

[15] G. Burkard, M. J. Gullans, X. Mi, and J. R. Petta, *Nature Reviews Physics* **2**, 129 (2020).

[16] C. W. Chou, H. de Riedmatten, D. Felinto, S. V. Polyakov, S. J. van Enk, and H. J. Kimble, *Nature* **438**, 828 (2005).

[17] D. N. Matsukevich, T. Chanelière, S. D. Jenkins, S.-Y. Lan, T. A. B. Kennedy, and A. Kuzmich, *Physical Review Letters* **96**, 030405 (2006).

[18] D. L. Moehring, P. Maunz, S. Olmschenk, K. C. Younge, D. N. Matsukevich, L.-M. Duan, and C. Monroe, *Nature* **449**, 68 (2007).

[19] S. Ritter, C. Nlleke, C. Hahn, A. Reiserer, A. Neuzner, M. Uphoff, M. McKe, E. Figueroa, J. Bochmann, and G. Rempe, *Nature* **484**, 195 (2012).

[20] S. T. Yilmaz, P. Fallahi, and A. Imamoğlu, *Physical Review Letters* **105**, 033601 (2010).

[21] I. Usmani, C. Clausen, F. Bussières, N. Sangouard, M. Afzelius, and N. Gisin, *Nature Photonics* **6**, 234 (2012).

[22] H. Bernien, B. Hensen, W. Pfaff, G. Koolstra, M. S. Blok, L. Robledo, T. H. Taminiau, M. Markham, D. J. Twitchen, L. Childress, and R. Hanson, *Nature* **497**, 86 (2013).

[23] A. Narla, S. Shankar, M. Hatridge, Z. Leghtas, K. Sliwa, E. Zalys-Geller, S. Mundhada, W. Pfaff, L. Frunzio, R. Schoelkopf, and M. Devoret, *Physical Review X* **6**, 031036 (2016).

[24] R. Riedinger, S. Hong, R. A. Norte, J. A. Slater, J. Shang, A. G. Krause, V. Anant, M. Aspelmeyer, and S. Grblacher, *Nature* **530**, 313 (2016).

[25] R. Riedinger, A. Wallucks, I. Marinković, C. Lschnauer, M. Aspelmeyer, S. Hong, and S. Grblacher, *Nature* **556**, 473 (2018).

[26] B. Hensen, H. Bernien, A. E. Dréau, A. Reiserer, N. Kalb, M. S. Blok, J. Ruitenberg, R. F. L. Vermeulen, R. N. Schouten, C. Abellán, W. Amaya, V. Pruneri, M. W. Mitchell, M. Markham, D. J. Twitchen, D. Elkouss, S. Wehner, T. H. Taminiau, and R. Hanson, *Nature* **526**, 682 (2015).

[27] A. Tchekbotareva, S. L. N. Hermans, P. C. Humphreys, D. Voigt, P. J. Harmsma, L. K. Cheng, A. L. Verlaan, N. Dijkhuizen, W. de Jong, A. Dréau, and R. Hanson, *Physical Review Letters* **123**, 063601 (2019).

[28] G. Murta, S. B. van Dam, J. Ribeiro, R. Hanson, and S. Wehner, *Quantum Science and Technology* **4**, 035011 (2019).

[29] G. Brassard, N. Lütkenhaus, T. Mor, and B. C. Sanders, *Physical Review Letters* **85**, 1330 (2000).

[30] J. Yin, Y. Cao, Y.-H. Li, S.-K. Liao, L. Zhang, J.-G. Ren, W.-Q. Cai, W.-Y. Liu, B. Li, H. Dai, G.-B. Li, Q.-M. Lu, Y.-H. Gong, Y. Xu, S.-L. Li, F.-Z. Li, Y.-Y. Yin, Z.-Q. Jiang, M. Li, J.-J. Jia, G. Ren, D. He, Y.-L. Zhou, X.-X. Zhang, N. Wang, X. Chang, Z.-C. Zhu, N.-L. Liu, Y.-A. Chen, C.-Y. Lu, R. Shu, C.-Z. Peng, J.-Y. Wang, and J.-W. Pan, *Science* **356**, 1140 (2017).

[31] T. Wilk, S. C. Webster, A. Kuhn, and G. Rempe, *Science* **317**, 488 (2007).

[32] B. Hacker, S. Welte, G. Rempe, and S. Ritter, *Nature* **536**, 193 (2016).

[33] O. Benson, C. Santori, M. Pelton, and Y. Yamamoto, *Physical Review Letters* **84**, 2513 (2000).

[34] D. Fattal, K. Inoue, J. Vučković, C. Santori, G. S. Solomon, and Y. Yamamoto, *Physical Review Letters* **92**, 037903 (2004).

[35] R. M. Stevenson, R. J. Young, P. Atkinson, K. Cooper, D. A. Ritchie, and A. J. Shields, *Nature* **439**, 179 (2006).

[36] N. Akopian, N. H. Lindner, E. Poem, Y. Berlatzky, J. Avron, D. Gershoni, B. D. Gerardot, and P. M. Petroff, *Physical Review Letters* **96**, 130501 (2006).

[37] H. Jayakumar, A. Predojević, T. Huber, T. Kauten, G. S. Solomon, and G. Weihs, *Physical Review Letters* **110**, 135505 (2013).

[38] H. Jayakumar, A. Predojević, T. Kauten, T. Huber, G. S.

Solomon, and G. Weihs, *Nature Communications* **5**, 4251 (2014).

[39] D. Huber, M. Reindl, S. F. C. da Silva, C. Schimpf, J. Martín-Sánchez, H. Huang, G. Piredda, J. Edlinger, A. Rastelli, and R. Trotta, *Physical Review Letters* **121**, 033902 (2018).

[40] M. Reindl, D. Huber, C. Schimpf, S. F. C. da Silva, M. B. Rota, H. Huang, V. Zwillaer, K. D. Jns, A. Rastelli, and R. Trotta, *Science Advances* **4**, eaau1255 (2018).

[41] Y. Chen, M. Zopf, R. Keil, F. Ding, and O. G. Schmidt, *Nature Communications* **9**, 2994 (2018).

[42] M. Prilmüller, T. Huber, M. Mller, P. Michler, G. Weihs, and A. Predojević, *Physical Review Letters* **121**, 110503 (2018).

[43] F. B. Basset, M. B. Rota, C. Schimpf, D. Tedeschi, K. D. Zeuner, S. F. C. da Silva, M. Reindl, V. Zwillaer, K. D. Jns, A. Rastelli, and R. Trotta, *Physical Review Letters* **123**, 160501 (2019).

[44] H. Wang, H. Hu, T.-H. Chung, J. Qin, X. Yang, J.-P. Li, R.-Z. Liu, H.-S. Zhong, Y.-M. He, X. Ding, Y.-H. Deng, Q. Dai, Y.-H. Huo, S. Hffing, C.-Y. Lu, and J.-W. Pan, *Physical Review Letters* **122**, 113602 (2019).

[45] J. Liu, R. Su, Y. Wei, B. Yao, S. F. C. da Silva, Y. Yu, J. Iles-Smith, K. Srinivasan, A. Rastelli, J. Li, and X. Wang, *Nature Nanotechnology* **14**, 586 (2019).

[46] S. Ding, G. Maslennikov, R. Hablitzel, H. Loh, and D. Matsukevich, *Physical Review Letters* **119**, 150404 (2017).

[47] S. Ding, G. Maslennikov, R. Hablitzel, and D. Matsukevich, *Physical Review Letters* **121**, 130502 (2018).

[48] S. Gasparinetti, M. Pechal, J.-C. Besse, M. Mondal, C. Eichler, and A. Wallraff, *Physical Review Letters* **119**, 140504 (2017).

[49] N. E. Frattini, V. V. Sivak, A. Lingenfelter, S. Shankar, and M. H. Devoret, *Physical Review Applied* **10**, 054020 (2018).

[50] M. Khoshnegar, T. Huber, A. Predojević, D. Dalacu, M. Prilmller, J. Lapointe, X. Wu, P. Tamarat, B. Lounis, P. Poole, G. Weihs, and H. Majedi, *Nature Communications* **8**, 15716 (2017).

[51] F. Wolf, C. Shi, J. C. Heip, M. Gessner, L. Pezzè, A. Smerzi, M. Schulte, K. Hammerer, and P. O. Schmidt, *Nature Communications* **10**, 2929 (2019).

[52] I. Straka, A. Predojević, T. Huber, L. Lachman, L. Butscek, M. Miková, M. Mičuda, G. S. Solomon, G. Weihs, M. Ježek, and R. Filip, *Physical Review Letters* **113**, 223603 (2014).

[53] A. Predojević, M. Ježek, T. Huber, H. Jayakumar, T. Kauten, G. S. Solomon, R. Filip, and G. Weihs, *Optics Express* **22**, 4789 (2014).

[54] R. Filip and L. Lachman, *Physical Review A* **88**, 043827 (2013).

[55] H. P. Yuen, *Physical Review A* **13**, 2226 (1976).

[56] C. Weedbrook, S. Pirandola, R. García-Patrón, N. J. Cerf, T. C. Ralph, J. H. Shapiro, and S. Lloyd, *Reviews of Modern Physics* **84**, 621 (2012).

[57] R. Filip and L. Mišta, *Physical Review Letters* **106**, 200401 (2011).

[58] M. B. Rota, F. B. Basset, D. Tedeschi, and R. Trotta, *IEEE Journal of Selected Topics in Quantum Electronics*, **1** (2020).

[59] L. Lachman and R. Filip, *Physical Review A* **88**, 063841 (2013).

[60] P. J. Mosley, J. S. Lundeen, B. J. Smith, P. Wasylczyk, A. B. U'Ren, C. Silberhorn, and I. A. Walmsley, *Physical Review Letters* **100**, 133601 (2008).

[61] D. B. Higginbottom, L. Slodička, G. Araneda, L. Lachman, R. Filip, M. Hennrich, and R. Blatt, *New Journal of Physics* **18**, 093038 (2016).

[62] K. Makino, Y. Hashimoto, J. ichi Yoshikawa, H. Ohdan, T. Toyama, P. van Loock, and A. Furusawa, *Science Advances* **2**, e1501772 (2016).

[63] Y. Y. Gao, B. J. Lester, Y. Zhang, C. Wang, S. Rosenblum, L. Frunzio, L. Jiang, S. Girvin, and R. J. Schoelkopf, *Physical Review X* **8**, 021073 (2018).

[64] L. Lachman, I. Straka, J. Hloušek, M. Ježek, and R. Filip, *Physical Review Letters* **123**, 043601 (2019).

[65] Y. Chu, P. Kharel, T. Yoon, L. Frunzio, P. T. Rakich, and R. J. Schoelkopf, *Nature* **563**, 666 (2018).

[66] L. R. Sletten, B. A. Moores, J. J. Viennot, and K. W. Lehnert, *Physical Review X* **9**, 021056 (2019).

[67] Y. Y. Gao, B. J. Lester, K. S. Chou, L. Frunzio, M. H. Devoret, L. Jiang, S. M. Girvin, and R. J. Schoelkopf, *Nature* **566**, 509 (2019).

[68] A. Kuhn, M. Hennrich, and G. Rempe, *Physical Review Letters* **89**, 067901 (2002).

[69] P. Lodahl, A. F. van Driel, I. S. Nikolaev, A. Irman, K. Overgaag, D. Vanmaekelbergh, and W. L. Vos, *Nature* **430**, 654 (2004).

[70] E. Peter, P. Senellart, D. Martrou, A. Lemaître, J. Hours, J. M. Gérard, and J. Bloch, *Physical Review Letters* **95**, 067401 (2005).

[71] X.-L. Chu, S. Gtzinger, and V. Sandoghdar, *Nature Photonics* **11**, 58 (2016).

I. SUPPLEMENTAL MATERIAL

A. Gaussian states

Unitary transformations of Gaussian states occupying n modes are conveniently described by transformation of the covariance matrix $\mathbf{\Gamma}$ and the vector of the first moments \mathbf{V} . The covariance matrix has elements

$$\begin{aligned}\Gamma_{2i-1,2j-1} &= \frac{1}{2}(\langle X_i X_j \rangle + \langle X_j X_i \rangle) - \langle X_i \rangle \langle X_j \rangle \\ \Gamma_{2i,2j} &= \frac{1}{2}(\langle P_i P_j \rangle + \langle P_j P_i \rangle) - \langle P_i \rangle \langle P_j \rangle \\ \Gamma_{2i-1,2j} &= \frac{1}{2}(\langle X_i P_j \rangle + \langle P_j X_i \rangle) - \langle X_i \rangle \langle P_j \rangle \\ \Gamma_{2i,2j-1} &= \frac{1}{2}(\langle P_i X_j \rangle + \langle X_j P_i \rangle) - \langle P_i \rangle \langle X_j \rangle, \quad (17)\end{aligned}$$

where i, j index the considered modes, X_i is the coordinate operator and P_i is the momentum operator. The vector \mathbf{V} has elements

$$\begin{aligned}V_{2i-1} &= \langle X_i \rangle \\ V_{2i} &= \langle P_i \rangle. \quad (18)\end{aligned}$$

The covariance matrix together with the vector \mathbf{V} specify any Gaussian state.

The unitary operations preserving the Gaussian aspects of Gaussian states are squeezing $S(V)$, rotation of the coordinates $\mathbf{R}(\phi)$, the beam splitter transformation

$U_{BS}(\tau)$ and displacement $\mathbf{D}(\alpha)$. The squeezing $\mathbf{S}^{(i)}$ of the coordinate X_i in the i th mode is described by

$$\begin{aligned} S_{2i-1,2i-1}^{(i)} &= \exp(-|\xi|) \\ S_{2i,2i}^{(i)} &= \exp(|\xi|) \end{aligned} \quad (19)$$

and $S_{m,n}^{(i)} = \delta_{m,n}$ otherwise. The matrix elements of $\mathbf{R}^{(i)}(\phi)$ acting on the i th mode are expressed as

$$\begin{aligned} R_{2i-1,2i-1}^{(i)} &= R_{2i,2i} = \cos \phi \\ R_{2i-1,2i}^{(i)} &= -R_{2i,2i-1} = \sin \phi \end{aligned} \quad (20)$$

and $R_{m,n}^{(i)} = \delta_{m,n}$ otherwise. The general squeezing operator $\mathbf{S}(\xi)$ acting on the i th mode is determined by

$$\mathbf{S}^{(i)}(\xi) = \mathbf{R}^{(i)}(-2\phi) \mathbf{S}^{(i)}(|\xi|) \mathbf{R}^{(i)}(2\phi), \quad (21)$$

where $\xi = |\xi| e^{i\phi}$. Further, the matrix $\mathbf{U}_{BS}^{(i,j)}(\tau)$ transforming the modes i and j is

$$\begin{aligned} U_{BS,2i-1,2i-1}^{(i,j)} &= U_{BS,2i,2i}^{(i,j)} = \sqrt{\tau} \\ U_{BS,2j-1,2j-1}^{(i,j)} &= U_{BS,2j,2j}^{(i,j)} = \sqrt{\tau} \\ U_{BS,2i-1,2j-1}^{(i,j)} &= U_{BS,2i,2j}^{(i,j)} = \sqrt{1-\tau} \\ U_{BS,2j-1,2i-1}^{(i,j)} &= U_{BS,2j,2i}^{(i,j)} = -\sqrt{1-\tau} \end{aligned} \quad (22)$$

and $U_{BS,m,n}^{(i,j)} = \delta_{m,n}$ otherwise. The displacement operator does not affect the covariance matrix but only the vector \mathbf{V} . Therefore, the displacement is represented formally by a vector

$$\mathbf{D}(\alpha) = (|\alpha_1| \cos \psi_1, |\alpha_1| \sin \psi_1, \dots, |\alpha_n| \cos \psi_n, |\alpha_n| \sin \psi_n) \quad (23)$$

which carries out transformation

$$\mathbf{V} = \tilde{\mathbf{V}} + \mathbf{\Gamma} \mathbf{D}, \quad (24)$$

where $\tilde{\mathbf{V}}$ is the vector of the first moments before an action of the displacement operator.

The covariance matrix of a general state $|G\rangle$ propagating through the setup in Fig. 1a) of the main text is determined by

$$\begin{aligned} \mathbf{\Gamma} &= \mathbf{U}_{BS}^{(1,2)}(1/2) \mathbf{U}_{BS}^{(3,4)}(1/2) \mathbf{U}_{BS}^{(2,3),T}(\tau) \mathbf{S}^{(2)}(\xi_2) \mathbf{S}^{(1)}(\xi_1) \cdot \\ &\quad \mathbb{I} \cdot \mathbf{S}^{(1),T}(\xi_1) \mathbf{S}^{(2),T}(\xi_2) \mathbf{U}_{BS}^{(2,3),T}(\tau) \\ &\quad \mathbf{U}_{BS}^{(3,4),T}(1/2) \mathbf{U}_{BS}^{(1,2),T}(1/2), \end{aligned} \quad (25)$$

where the superscript T denotes the transposition of the matrix. The first moments yield

$$\mathbf{V}^T = \mathbf{U}_{BS}^{(1,2)}(1/2) \mathbf{U}_{BS}^{(3,4)}(1/2) \tilde{\mathbf{V}} \mathbf{\Gamma} \mathbf{D}^T(\alpha) \quad (26)$$

with

$$\begin{aligned} \tilde{\mathbf{V}} &= \mathbf{U}_{BS}^{(2,3),T}(\tau) \mathbf{S}^{(2)}(\xi_2) \mathbf{S}^{(1)}(\xi_1) \cdot \\ &\quad \mathbb{I} \cdot \mathbf{S}^{(1),T}(\xi_1) \mathbf{S}^{(2),T}(\xi_2) \mathbf{U}_{BS}^{(2,3),T}(\tau) \end{aligned} \quad (27)$$

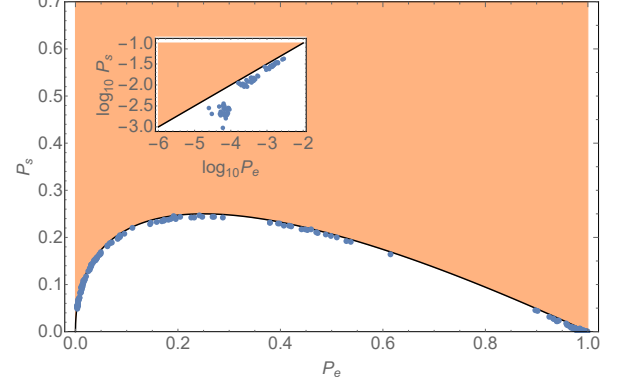


FIG. 3. Figure depicts results of a Monte - Carlo simulation randomly producing probabilities $P_{1,1}$, $P_{e,1} = 1 - P_0^{(1)} - P_0^{(2)}$ and $P_{e,2} = 1 - P_1^{(2)} - P_1^{(1)}$ exhibited by Gaussian states when a PNRD is used for detection. The inset shows the results of experimentally relevant region of states with very low error probabilities. The black solid line corresponds to the threshold covering all the states. The blue points represent fifty points generated in the Monte-Carlo simulation that get closer to the threshold. A total number of cycles in the simulation was 10^6 for each parameter of squeezing in a single mode.

and

$$\mathbf{D} = (|\alpha_1| \cos \psi_1, |\alpha_1| \sin \psi_1, |\alpha_2| \cos \psi_2, |\alpha_2| \sin \psi_2, 0, 0, 0, 0, 0). \quad (28)$$

Projection on the vacuum in one or more modes is given by [56]

$$P_{\mathbf{M}} = \frac{\exp\left[\frac{\mathbf{V}(\mathbf{\Gamma} + \mathbf{M})^{-1} \mathbf{V}^T - \mathbf{V} \mathbf{\Gamma} \mathbf{V}^T}{2}\right]}{\sqrt{\det(\mathbf{\Gamma} + \mathbf{M})}} \quad (29)$$

with \mathbf{M} being a matrix determining the measurement with elements $M_{i,j} = \delta_{i,j} m_i$, where $m_{2k-1} = m_{2k} = 1$ if the projection is carried out in the k th mode and otherwise $m_{2k-1} = m_{2k} = 0$. For a simpler notation, let us introduce a vector $\mathbf{m} = (m_1, \dots, m_{2n})$ and distinguish the probabilities (29) by \mathbf{m} instead of \mathbf{M} . Then, the success and error probabilities employed in the main text are given by

$$\begin{aligned} P_s &= 1 - P_{(0,0,1,1,0,0,0,0)} - P_{(0,0,0,0,1,1,0,0)} + P_{(0,0,1,1,1,1,0,0)} \\ P_{e,1} &= 1 - 2P_{(0,0,1,1,0,0,0,0)} + P_{(1,1,1,1,0,0,0,0)} \\ P_{e,2} &= 1 - 2P_{(0,0,0,0,1,1,0,0)} + P_{(0,0,0,0,1,1,1,1)} \end{aligned} \quad (30)$$

The exact analytical expressions of those probabilities obtain very extensive forms.

The formulas can be modified for the response of a detector distinguishing a number of arriving photons. Two such detectors measuring different modes allow us to get the probabilities $P_{mn} = \langle m | \langle n | \rho | m \rangle | n \rangle$ for m and n up to some number. Let us work out the probability $P_{m,n}$ exhibited by Gaussian states. They are achieved from an

overlap of Wigner functions

$$P_{m,n} = 16\pi^2 \int W_m(x_1, p_1) W_n(x_2, p_2) \times \\ W_G(x_1, p_1, x_2, p_2) dx_1 dx_2 dp_1 dp_2, \quad (31)$$

where W_m stands for the Wigner function of the Fock state $|m\rangle$ and W_G denotes the Wigner function of a Gaussian state. Direct calculation of the integral (31) for a general Gaussian state in two modes gives rise to very extensive expressions, which are hard to manipulate analytically. Therefore, the solution of the integral is expressed in terms of derivation of the formula (29) according to the elements of the covariance matrix (17). Let us introduce an operator

$$\mathbf{L}_{M,i} = -1 - 2\partial_{\Gamma_{2i-1,2i-1}} - 2\partial_{\Gamma_{2i,2i}}, \quad (32)$$

where $\bar{\Gamma} = \Gamma + \mathbf{M}$ and i being 1 or 2 picks relevant elements of $\bar{\Gamma}$. The probabilities exposing the quantum non-Gaussian coincidences are expressed as

$$P_{1,1} = \mathbf{L}_{M,1} \mathbf{L}_{M,2} P_M(\Gamma) \\ P_1^{(i)} = \mathbf{L}_{M^{(i)},i} P_{M^{(i)}}(\Gamma) \\ P_0^{(i)} = \mathbf{L}_{M^{(i)},i} P_{M^{(i)}}(\Gamma), \quad (33)$$

where \mathbf{M} is an identity matrix of rank two, $\mathbf{M}^{(1)}$ has elements $M_{i,j}^{(1)} = \delta_{i,j} m_i$ with $m_1 = m_2 = 1$ and $m_3 = m_4 = 0$ and, finally, $\mathbf{M}^{(2)}$ has elements $M_{i,j}^{(2)} = \delta_{i,j} m_i$ with $m_1 = m_2 = 0$ and $m_3 = m_4 = 1$.

B. Monte-Carlo simulation

The thresholds, which are established by the state

$$|G\rangle_{1,2} = \sqrt{1-r^2} \sum_{n=0}^{\infty} r^n |n\rangle |n\rangle, \quad (34)$$

cover all two-mode Gaussian states in both detection schemes, where SPADs or PNRDs are employed. To certify this, we performed several Monte-Carlo simulations where random states $|G\rangle_{1,2}$ were generated. Each simulation was performed for one fixed squeezing operator generating the Gaussian state. Changing the parameter of the operator shifted a region where a Monte-Carlo simulation sets generated points. All the remaining unitary operators were produced randomly. We carried out ten simulations with fixed squeezing $\exp(-|\xi_1|) = \{0.1, 0.2, 0.3, 0.4, 0.5, 0.6, 0.7, 0.8, 0.9\}$ for both detection schemes. The others parameters were generated randomly in intervals $\exp(-|\xi_2|) \in (0, 1)$, $\phi \in (0, 2\pi)$, $\tau \in (0, 2\pi)$, $|\alpha_1| \in (0, 1.5)$, $|\alpha_2| \in (0, 1.5)$, $\psi_1 \in (0, 2\pi)$ and $\psi_2 \in (0, 2\pi)$. Fig. 2 in the main text presents the results for the measurement with SPADs and Fig. 3 shows the results when PNRDs are used. Since each simulation produced 10^6 states, the figures show only the best 50 attempts in each simulation. Because the simulations were carried out ten times with different fixed squeezing parameters in both measurements, each figure presents five hundred best attempts.

C. Model of realistic states

The model of a realistic source producing a photon pair has the form $\rho_{\eta,T} \otimes \rho_{\bar{n},1} \otimes \rho_{\bar{n},2}$ with

$$\rho_{\eta,T} = \eta T^2 |1\rangle_1 |1\rangle_2 \langle 1|_1 \langle 1|_2 \\ + \eta T (1-T) (|1\rangle_1 |0\rangle_2 \langle 1|_1 \langle 0|_2 + |0\rangle_1 |1\rangle_2 \langle 0|_1 \langle 1|_2) \\ + [(1-\eta) + \eta(1-T)^2] |0\rangle_1 |0\rangle_2 \langle 0|_1 \langle 0|_2 \\ \rho_{\bar{n},i} = e^{-\bar{n}} \sum_{k=0}^{\infty} \frac{\bar{n}^k}{k!} |k\rangle_i \langle k|_i. \quad (35)$$

This state yields the probabilities of quantifying probability of projection to the vacuum

$$P_{(0,0,1,1,1,1,0,0)} = \left[1 - \eta + \eta \left(1 - \frac{T}{2} \right)^2 \right] e^{-\bar{n}/2} \\ P_{(0,0,1,1,0,0,0,0)} = P_{(0,0,0,0,1,1,0,0)} = (1 - \eta T/2) e^{-\bar{n}/2} \\ P_{(1,1,1,1,0,0,0,0)} = P_{(0,0,0,0,1,1,1,1)} = (1 - \eta T) e^{-\bar{n}}, \quad (36)$$

which allow us to express the success and error probabilities according to (30). When a photon-number resolving detector responds to the model state, the success and error probabilities become

$$P_s = [\eta T^2 + 2\eta\bar{n}T^2(1-T)] e^{-2T\bar{n}} \\ + [\bar{n}^2 T^2 (1 - \eta + \eta T) T^2 \bar{n}^2] e^{-2T\bar{n}} \\ P_{e,1} = P_{e,2} = 1 - \\ [1 - \eta T + (1 - \eta T) T \bar{n} + \eta T] e^{-2T\bar{n}}. \quad (37)$$

A condition imposed on the parameters that is required by the quantum non-Gaussian coincidences is presented in Fig. 4a) and b) for cases of employing SPADs or PNRDs.

Other experimental scenarios detect the quantum non-Gaussianity in a single mode, where the other mode is either ignored, or used for heralding. In the former case, the state $\rho_1 = \text{Tr}_2[\rho]$ works out to be

$$\rho_1 = [\eta T |1\rangle\langle 1| + (1 - \eta T) |0\rangle\langle 0|] \otimes \tilde{\rho}_1(T\bar{n}). \quad (38)$$

When the state is prepared conditionally by heralding, the density matrix reads

$$\rho_1 = \frac{1}{N} \text{Tr}_2 \{ [|1\rangle\langle 1| \otimes |0\rangle\langle 0| + \mathbb{I} \otimes (\mathbb{I} - |0\rangle\langle 0|)] \rho \} \quad (39)$$

with N being a probability of the heralding. An explicit form of the heralded state is

$$\rho_1 = \frac{1}{N} \{ [(1 - \eta T)(1 - e^{-T\bar{n}}) + \eta T(1 - T)e^{-T\bar{n}}] |0\rangle\langle 0| \\ + \eta T e^{-T\bar{n}} (-1 + e^{T\bar{n}} + T) |1\rangle\langle 1| \} \otimes \tilde{\rho}_1(T\bar{n}), \quad (40)$$

where $N = 1 - e^{-T\bar{n}} + e^{-T\bar{n}} \eta T$. Fig. 4 c) and d) present manifestation of the quantum non-Gaussianity in a single mode by states (38) and (40).

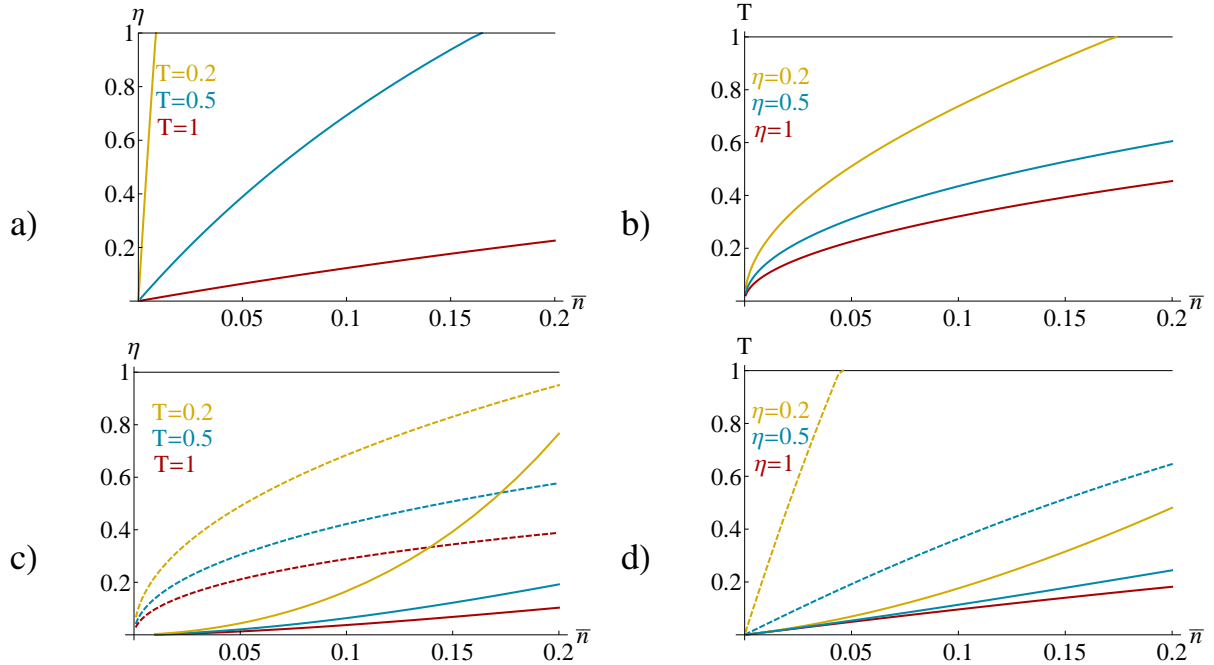


FIG. 4. Figures present quantum non-Gaussian coincidences and quantum non-Gaussianity exhibited by the state $\rho_{\eta,T} \otimes \tilde{\rho}_1(T\bar{n}) \otimes \tilde{\rho}_2(T\bar{n})$ in different detection scenarios. a) Thresholds revealing the quantum non-Gaussian coincidences of the state for different losses T , which the colors distinguish. Whereas the solid lines correspond to conditions when SPADs are employed, the dashed lines represent the conditions for measurement with PNRDs. The quantum non-Gaussian states are above those lines. b) The solid lines represent robustness of the quantum non-Gaussian coincidences against losses for several parameters η using detection with SPADs. The dashed lines show the same thresholds when PNRDs are used. c) Employing the criterion in [59], the figure presents threshold parameters for the quantum non-Gaussianity of the heralded state (solid) and unheralded state (dashed). The colors differentiate losses T again. d) An analysis regarding the robustness against losses of the quantum non-Gaussian test for the heralded state (solid) and unheralded state (dashed). The colors distinguish probability of the photon-pair emission η . The robustness of both heralded and unheralded states is identical for $\eta = 1$.